Draft version December 17, 2025
Typeset using LaTeX **default** style in AASTeX7.0.1

The X-ray flare spectrum of HR 1099: the search for photopumped Ne IX line emission

Damian J. Christian [1], Francis P. Keenan,[2] Steven J. Rose,[3] and Katja Poppenhaeger[4]

[1] *Department of Physics and Astronomy, California State University Northridge, Northridge, CA 91330, USA*
[2] *Astrophysics Research Centre, School of Mathematics and Physics, Queen's University Belfast, Belfast BT7 1NN, UK*
[3] *Department of Physics, Imperial College London, London SW7 2AZ, UK*
[4] *Leibniz Institute for Astrophysics Potsdam, 14482 Potsdam, Germany*

ABSTRACT

We present high resolution X-ray spectroscopy of the active late-type star HR 1099 obtained with the Chandra Low Energy Transmission Grating (LETG) Spectrometer. A spectrum extracted from the early stages of a flare was created to search for enhanced emission due to line coincidence photopumping at X-ray wavelengths, rather than the usual optical and ultraviolet cases. Specifically, we have identified a scheme where a He-like Ne IX line at 11 Å is photopumped by He-like Na X, which predicts intensity enhancement in the Ne IX 82.76 Å transition under the high electron density and large coronal pathlength conditions found in stellar and solar flares. We previously tentatively identified a Ne IX enhancement in a solar flare spectrum, but the result was extremely uncertain. However, Ne IX 82.76 Å was detected at the 3-sigma level in the Chandra spectrum, leading to a measured Ne IX 82.76/13.45 intensity ratio of 0.21±0.08. By contrast, the theoretical ratio from the CHIANTI database is at most 0.031, indicating an enhancement factor of at least 7±3 for the 82.76 Å line, in agreement with the expected value of ∼7–15 from a photopumping plasma model. This confirms detection, for the first time to our knowledge, of X-ray photopumping in an astrophysical object. We note that the identification of such X-ray photopumping in other spatially-unresolved sources provides in principle a new diagnostic for independently determining the sizes of their coronal regions.

Keywords: Flare Stars (540) – Spectroscopy (1558) – X-ray stars (1823) – stars:individual:HR 1099

1. INTRODUCTION

Bowen (1934) was the first to identify line coincidence photopumping in an astrophysical source. In this mechanism, line emission from a species is coincident in wavelength with a transition in another species, leading to radiative excitation in the latter. The photopumping scheme of Bowen – termed Bowen fluorescence – involves He II lines at 303.80 Å pumping O III transitions at this wavelength, as a consequence of which several O III features are observed to be much stronger than would otherwise be expected in a nebular plasma. Since the work of Bowen, many other cases of photopumping in astrophysical objects have been found (see the review by Hartman (2013)), although these all involve lowly ionized species, and to our knowledge there has been no detection of photopumping in a high temperature (coronal) source.

However, Keenan et al. (2018) identified a scheme in the X-ray regime (modelled by Nilsen & Chandler (1991) for laboratory plasmas), whereby a He-like line of Ne IX at 11.000 Å was photopumped by He-like Na X at 11.003 Å, leading to intensity enhancement in the Ne IX 82.76 Å transition. We present the energy level diagram from Keenan et al. (2018) in Figure 1. This enhancement was predicted to be possibly detectable under physical conditions found in solar flare loops, albeit at the extreme limits of plasma electron density and pathlength. An unidentified feature at 82.76 Å in the soft X-ray rocket spectrum of a solar flare obtained by Acton et al. (1985) appeared to be the Ne IX line, especially as its apparent intensity enhancement factor of ∼5 was not too different from the expected theoretical value of ∼2. Unfortunately, although this result was encouraging, the flare spectrum of Acton et al. (1985), recorded

Corresponding author: Damian J. Christian
damian.christian@csun.edu

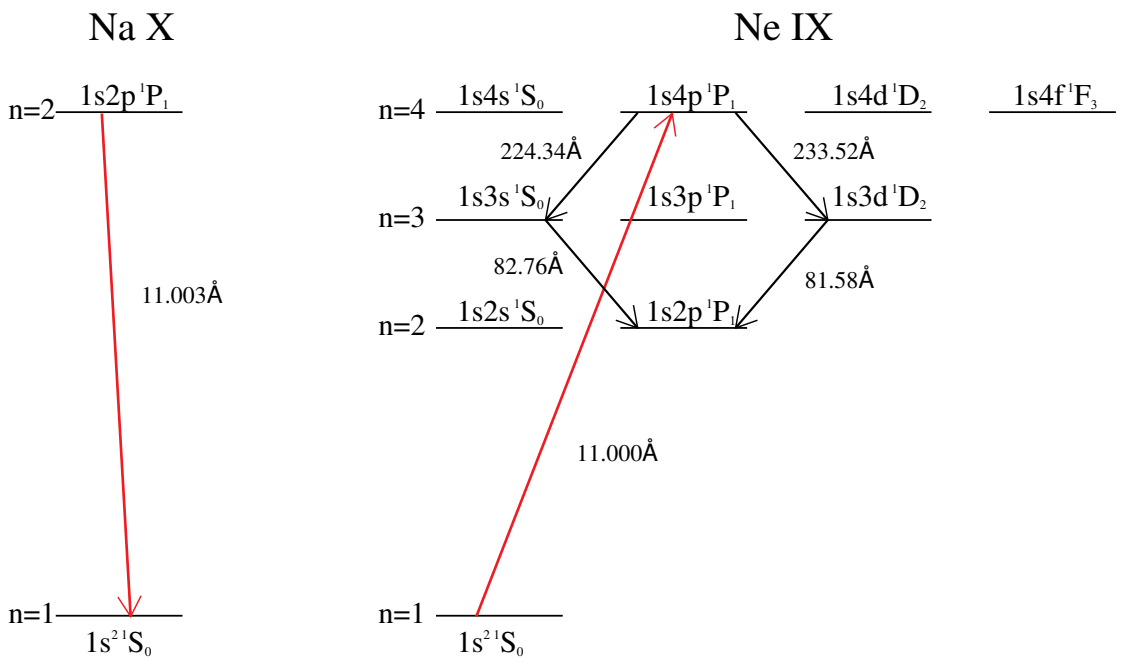

Figure 1. Energy level diagrams for Na X and Ne IX showing the X-ray photopumping scheme (reproduced with permission from Keenan et al. (2018)). The $1s^2\ ^1S_0$–$1s4p\ ^1P_1$ transition of Ne IX at 11.000 Å is photopumped by the $1s^2\ ^1S_0$–$1s2p\ ^1P_1$ resonance line of Na X at 11.003 Å. Subsequently, the electrons in $1s4p\ ^1P_1$ decay to $1s3s\ ^1S_0$ or $1s3d\ ^1D_2$, producing the 224.34 Å and 233.52 Å emission lines, respectively, which in turn both decay to $1s2p\ ^1P_1$, producing 82.76 Å and 81.58 Å, respectively. However the enhancement in the 81.58 Å line is predicted to be a factor of 20 smaller than for 82.76 Å.

on photographic emulsion, was no longer accessible and hence the quality of their 82.76 Å intensity measurement could not be further investigated and assessed. Hence the detection of Ne IX photopumping remains extremely marginal at best. Indeed, previously Keenan et al. (2006) have identified the line in the Action et al. spectrum as being due to Fe XV.

Clearly, further flare observations of the Ne IX 82.76 Å line are highly desirable, to confirm the findings of Keenan et al. (2018), and not just because it is an interesting plasma effect. The degree of line intensity enhancement depends on the electron density N_e and pathlength L of the emitting plasma, and using diagnostic line ratios to determine N_e would therefore allow an independent measurement of L. This would have important applications for unresolved stellar sources, where the methods for determining L in flaring loops requires various assumptions to be made (Mullan et al. 2006). However, the spectral region covering the 82.76 Å transition is relatively unexplored in terms of solar observations, and no suitable datasets exist.

Fortunately, the Ne IX transition lies within the wavelength range (1.2–175 Å) of the Low Energy Transmission Grating (LETG) of the Chandra satellite (Brinkman et al. 2000). Furthermore, the coronae of late-type stars have large electron density and pathlength flaring loops (Mullan et al. 2006), as well as high flare rates (Hilton et al. 2010), which should make the detection of line enhancement more likely than for a solar flare. We have hence undertaken a search of the Chandra archive for flare spectra of late-type stars that are good candidates for detecting Ne IX 82.76 Å line enhancement. Our paper is organised as follows. In Section 2 we present the Chandra observations and their reduction and analysis, along with our line intensity measurements. Section 3 provides a brief summary of our line enhancement calculations and generation of theoretical spectra for comparison with observations. Finally, in Section 4 we discuss our results and possible future work.

Table 1. Chandra LETG archival stellar data

Star	OBS ID	Obs. Date	Exp. Time (ksec)
HR 1099	1879	2001-01-10T23:14:49	94.9

2. CHANDRA OBSERVATIONS

We selected over 20 known flare stars from the Chandra Archive [1] that were observed with the High Resolution Camera (HRC) and LETG. This set-up provides the necessary 1 to ≈175 Å range to cover the emission lines of interest. Flares (with peak flare emission $\gtrsim$2 times the quiescent level) were selected from the HRC + LETG observations of AB Dor, AD Leo, AU Mic, HR 1099, VW Cep, Xi Boo and YY Gem. LETG spectra were extracted from the flare intervals of each flaring star. The January 2001 observation of HR 1099 was the most promising candidate with a large flare, and the observing details are summarized in Table 1. This star, also known as V711 Tau and HD 22468, is an RS CVn binary and active system that has been extensively studied in the X-ray region since the HEAO-1 observations of Walter et al. (1978). Subsequently, there have been high resolution X-ray grating observations of HR 1099, such as XMM RGS measurements of elemental abundances (Brinkman et al. 2001) and Chandra LETG coronal density diagnostics (Ness et al. 2002). We show the HR 1099 0th-order light curve in Fig. 2.

The HR 1099 data were analyzed with the latest version of the Chandra Interactive Analysis of Observations (CIAO 4.16; Fruscione et al. (2006)). A light curves was created using CIAO software from the 0th-order image, and spectra extracted for the flare interval derived from the light curve (18.6 ksec). A non-flaring spectrum of "quiet" emission was also extracted for HR 1099 from non-flaring times where the count rate was below ≈1.6 cps (76.6 ksec exposure). The extracted spectra were fitted with Sherpa and multi-Gaussian emission line models, and we combined the "plus" and "minus" LETG orders to increase the signal-to-noise. Care was taken to align the orders and the +1 order was shifted by +0.0375 Å to match the −1 order based on the peak wavelengths of the strongest emission lines. We note that the Chandra Proposers' Observatory Guide (Section 9.3.3[2]) states that the true LETG instrumental profile is a Moffat function. However, we have compared our Gaussian line fits for the strongest lines to Moffat profiles and find they are consistent, in agreement with previous studies (Hussain et al. 2007). The LETG spectrum was then separated into four main regions for line fitting: 5–40, 40–80, 80–120, and 120–165 Å. Standard background subtraction was applied to each of these spectral regions. Each of spectral regions was fit with a model consisting of multiple individual emission lines and a variable continuum. The wavelength of each individual emission line was fixed at the laboratory values for the initial fitting and then allowed to vary by up to ±0.05 Å. The continuum was modeled as a power-law and allowed to be free, while the 5–40 Å region was binned by a factor of 2 and the other three by a factor of 4. This gives a line spread function (LSP) of 0.025 Å in the 5–40 Å region and 0.05 Å in the others. We note this is ≈3 to 4 times smaller than the LSP when grouping by signal-to-noise ratio, which includes more bins and has a wider LSP. Line widths (σ) were fixed at 0.02 Å for the 5–40 Å region and 0.04 Å for the others, apart from 40–50 Å where they were ≈3 to 4 times larger. In general, the reduced χ^2 was < 1 for all four spectral regions for the flare and quiescent spectra. For the flare spectra χ^2 over the degrees of freedom were: 936/1334 for the 5–40 Å region, 450/642 for 40–80 Å, 550/788 for 80–120 Å, and 664/892 for 120–165 Å. In Fig. 3 we show the complete sample flare spectrum, covering 5–165 Å.

The HR 1099 flare intensity increased by about a factor of 1.8 above the quiescent emission, with the former having a flux of 3.2×10^{-10} ergs cm^{-2} s^{-1} (luminosity 3.3×10^{31} ergs s^{-1}), compared to the quiescent value of 1.8×10^{-10} ergs cm^{-2} s^{-1} (luminosity 1.8×10^{31} ergs s^{-1}) in the 0.07–2.5 keV range. This luminosity is similar to, but slightly higher than, the Testa et al. (2004) value for HR 1099 from their Chandra High Energy Transmission Grating (HETG) observations.

We fitted the LETG flare spectrum in the 5–165 Å region, and detected many of the strong emission lines previously observed in solar and stellar flares (Acton et al. 1985). Strong emission lines in the 5–40 Å range included: Ne X 12.15 Å, Fe XVII 17.06 Å, O VIII 18.97 Å and O VII 21.55 Å, while weaker transitions of Si XIV, Mg XII and Fe XIX were also detected. The significance of these measurements ranged from 2–8 sigma above the background. We detected a moderately strong emission line near 11.0 Å that we identify as the Ne IX/Na X blend (see Figure 3b), which has been previously observed to be of moderate strength in a solar flare (Phillips et al. 2010). Our measurements are summarized

[1] https://cxc.harvard.edu/cda/

[2] https://cxc.harvard.edu/proposer/POG/html/chap9.html

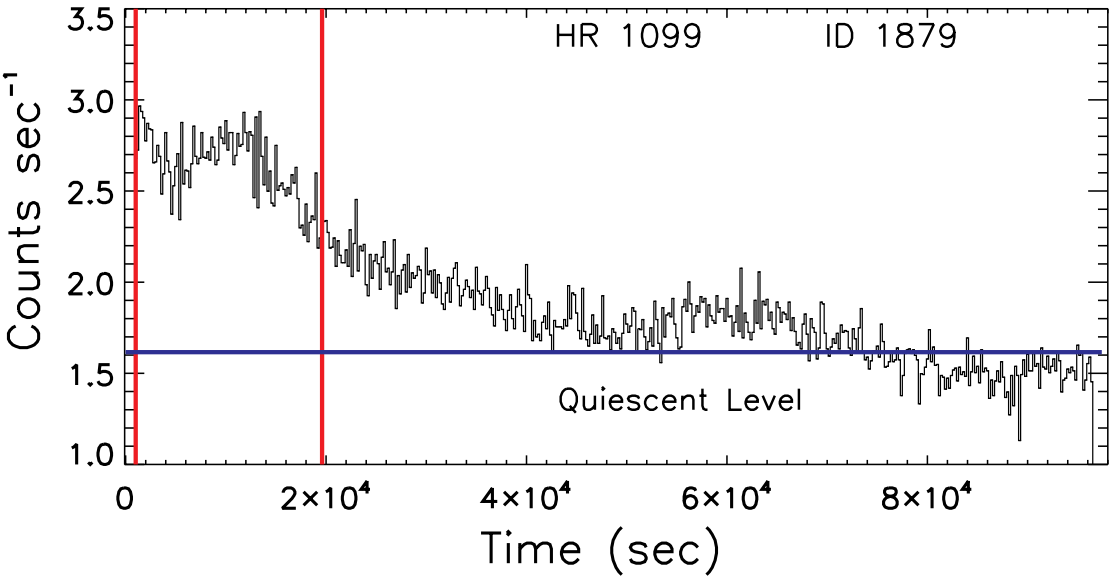

Figure 2. CXO LETG 0th-order light curve for HR 1099 in the 0.3–2.5 keV band. The flaring interval is indicated on the left between the red vertical lines, in the first 20 ksec of the observation from 10 January 2001. The bin size is 200 sec, and the quiescent level indicated by the blue horizontal line.

in Table 2, where we include line fluxes from both the flare and quiescent HR 1099 spectra for the strongest emission lines and lines important to this study, such as those used for density diagnostics. For weaker emission lines, upper-limits are denoted as $<$ and given as 3σ, i.e. 3 times the measured error. The instrument's aluminum edge near 44 Å and the detector gaps between 52 and 60 Å (for the -1 order) and 61.9 and 64.7 Å ($+1$ order) made the identification and measurement of lines in these regions difficult. However, in the slightly longer wavelength region, we find a strong line of C VI at 56.9 Å, and marginally detect the usually intense Fe XV line at 59.4 Å (Keenan et al. 2006) along with Fe XV 66.25 Å. There is a moderately strong line at 65.66 Å that we attribute to Mg X. As expected, other Fe XV lines in the 70–80 Å region previously identified by Keenan et al. (2006) in a solar flare were not detected. The longer wavelength region of the HR 1099 flaring spectrum also shows the strong lines of Fe XVIII 103.93 Å, Fe XXI 128.78 Å and Fe XXIII/Fe XX 132.92 Å. In addition, this region includes Fe XVIII 93.95 Å, known to be one of the more intense lines in solar flares (Kastner et al. 1974), and which has a dedicated channel in NASA's Solar Dynamic Observatory's Atmospheric Imaging Assembly (AIA; Lemen et al. (2012)). The intensity peak of Fe XVIII 93.95 Å is about 1.4 times higher in the flare spectrum than in the quiescent spectrum,

An inspection of Table 2 also reveals a listing for Ne IX 82.76 Å, which in addition is shown in Figs. 3c and 6. We discuss this detection in detail in Section 4.

3. LINE ENHANCEMENT FACTOR AND CHIANTI CALCULATION

The calculation of the expected enhancement in Ne IX lines due to photopumping is discussed in detail in Keenan et al. (2018) and hence will not be repeated here. However, we note that in these calculations, photopumping is only considered from the Na X 11.0 Å line, and not from any background continuum radiation, although the inclusion of this would lead to an enhanced effect. The results in Keenan et al. were generated for solar coronal abundances, appropriate to the analysis of the solar flare in that paper. We have therefore recalculated the Ne IX line enhancement factors (i.e. line intensity of the photopumped line divided by that when there is no pumping) using the measured HR 1099 coronal abundances of Huenemoerder et al. (2013), apart from data for Ni which was not considered by these authors and was taken from Nordon & Behar (2007). The factors are plotted in Fig 4 as a function of pathlength (L)

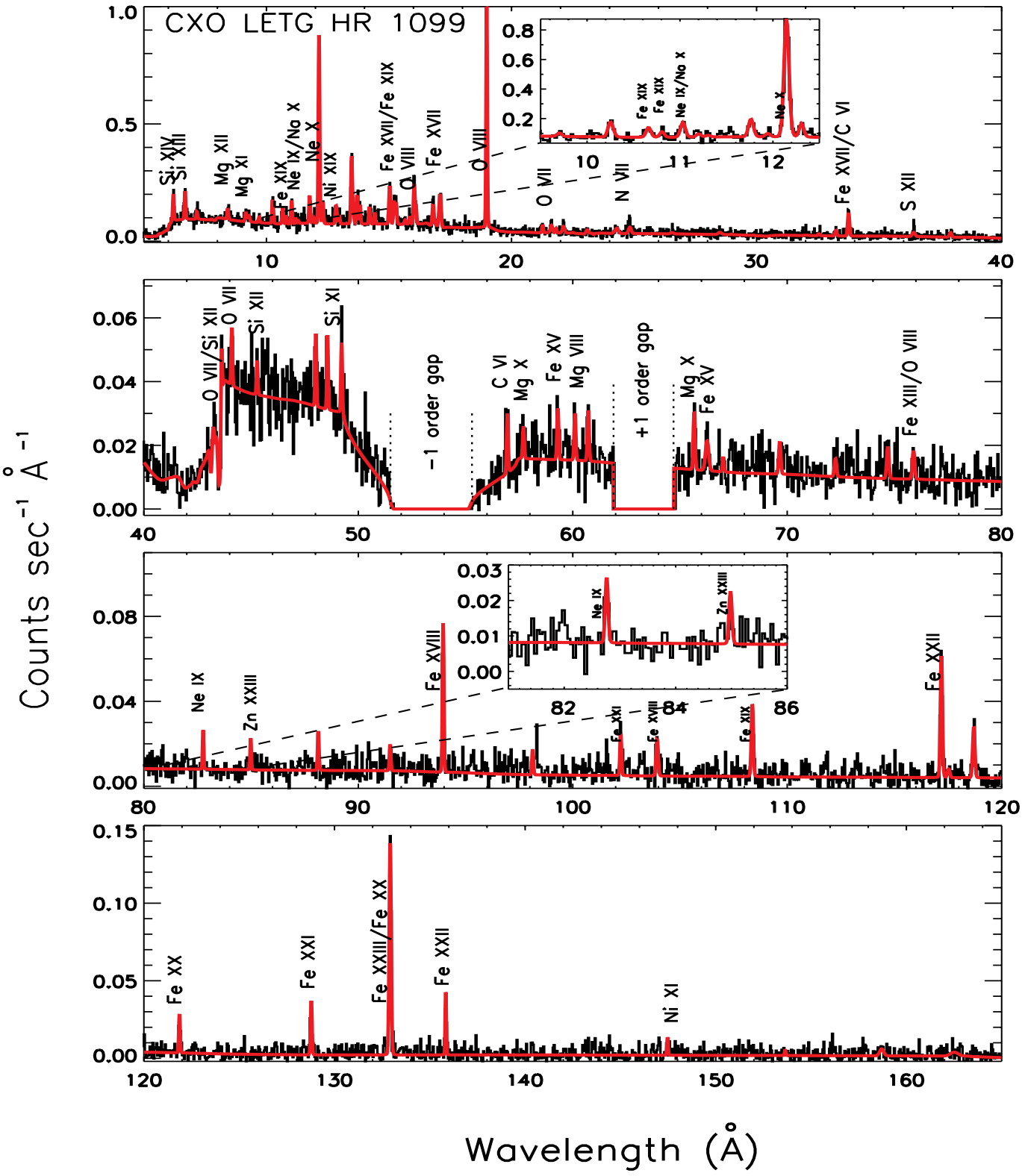

Figure 3. The LETG HR 1099 flare spectra. The upper panels show the entire 5–165 Å HR 1099 LETG flare spectrum in four spectral windows. The insets in the top (5–40 Å) and third (80–120 Å) panels show expanded spectral regions of interest. Data are plotted as a black histogram, and the best-fitting emission line model over-plotted as a red curve. Line identifications are indicated for some of the strongest emission features.

and electron density (N_e) for a range of L (= 10^9–10^{13} cm) and N_e (= 10^{10}–10^{14} cm^{-3}) appropriate to flaring coronal loops in active late-type stars (Mullan et al. 2006). We note that the results are far less sensitive to changes in the electron temperature T_e than N_e or L. For example, at log N_e = 12 and log L = 11, changing the temperature from that of maximum Ne IX fractional abundance in ionization equilibrium, log T_e = 6.2 (Bryans et al. (2009)), to log T_e = 6.4 leads to only a 25% change in the enhancement factor, from 5.5 to 4.1. Even at log T_e = 6.6 the factor is still 2.5. At very high temperatures the factor approaches 1.0, but this is only because at such large values of T_e there are no Ne IX ions remaining in the plasma model.

In addition to line enhancement calculations, we have generated synthetic spectra for HR 1099 to aid in our analysis of the Chandra data and investigating any potential blends. This was produced with Version 10.1 of the CHIANTI atomic database (Dere et al. 1997, 2023). Clearly, it would be inappropriate to compare the HR 1099 observations with a CHIANTI model for a solar flare. Instead, we have used the AU Mic emission measure distribution (EMD) option in CHIANTI (very approximately flat on a logarithmic scale from log T_e = 6.0 – 7.1), not too different to that for HR 1099 (Huenemoerder et al. 2013), and hence is the most appropriate CHIANTI model for such a highly active late-type star. However, to assess how sensitive our theoretical line intensities are to different models we have also calculated results for the flare EMD option in CHIANTI (very steeply rising on a logarithmic scale from log T_e = 6.0 – 7.2), plus the isothermal plasma case. The spectra were generated using the HR 1099 coronal abundances from Huenemoerder et al. (2013) and Nordon & Behar (2007) rather than the default solar values.

4. RESULTS AND DISCUSSION

As noted in Keenan et al. (2018), the detection of line enhancement during a stellar flare will provide measurements of physical parameters currently poorly constrained in these spatially-unresolved sources. Specifically, from a measurement of the degree of line enhancement the loop pathlength of the emitting plasma can be derived, once the electron density is known.

4.1. *Identification of the Ne IX 82.76 Å line*

We have identified an emission line at 82.76 Å in the Chandra spectrum, shown in Fig 5, with an intensity of (33.4 ± 11.9) × 10^{-5} ph cm^{-2} s^{-1}. However, previously Keenan et al. (2006) identified this line in the solar flare spectrum of Acton et al. (1985) as being due to Fe XV 83.23 Å, and hence it clearly needs a detailed assessment. First, we note that the wavelength of the Ne IX line has been accurately determined to be 82.76 ± 0.001 Å (Keenan et al. 2018), in agreement with the Acton et al. measurement, while the Fe XV transition only has an approximate theoretical wavelength of 83.23 Å. Most importantly, for the solar flare data analysed by Keenan et al. (2018), the Fe XV 83.23 Å/59.40 Å intensity ratio is 0.75, while the theoretical value is predicted to be only 0.37 for the flare electron density of log $N_e \simeq 10.5$ (Brown et al. 1986), indicating the presence of blends. This is further supported by the fact that Acton et al. note that the 82.76 Å feature is broad and hence a blend. We therefore conclude that the 82.76 Å line in the solar flare data is not solely due to Fe XV, but rather is a Ne IX/Fe XV blend.

Now considering the HR 1099 spectrum, we note that the theoretical Fe XV 83.23 Å/59.40 Å ratio ranges from 0.28 – 0.38, depending on which of the flare EMD, AU Mic EMD or isothermal models is adopted in CHIANTI. However, even for the maximum value of the line ratio of 0.38, the measured intensity of the Fe XV 59.40 Å transition in the HR 1099 spectrum indicates that 83.23 Å would make at most a 29% contribution to the 82.76 Å feature. The CHIANTI synthetic spectra also contain some other lines that blend with the Ne IX transition, but none is significant, with even Fe XII 82.74 Å predicted to contribute only about 16% to the total 82.76 Å intensity in the absence of photopumping, and hence much less if the line is enhanced. To be sure of our detection, we have in addition searched for other nearby features that could have been mistaken for Ne IX, even though their wavelength separations from 82.76 Å are greater than the Chandra LETG spectral resolution of 0.05 Å (FWHM). A Mg VIII line is predicted to lie at 82.82 Å, relatively close to 82.76 Å. However, CHIANTI calculates a Mg VIII 75.05 Å/82.82 Å line intensity ratio of 5, and the 75.05 Å line is not detected in the HR 1099 data, so 82.82 Å should not be present. In addition, there is Fe XII 82.67 Å, but this is calculated to be only 1.5% of the intensity of Fe XVIII 93.95 Å, i.e. 2.3 × 10^{-5} ph cm^{-2} s^{-1}, far smaller than our 82.76 Å measurement. Furthermore, there are no Fe XII lines in the Acton et al. spectrum, nor in ours. However, if the 82.76 Å feature were due to Fe XII 82.67 Å, one would expect to see Fe XII 79.48 Å, which is predicted to be close to 82.67 Å in intensity. Given all of the above, we are confident that the feature at 82.76 Å is due to Ne IX.

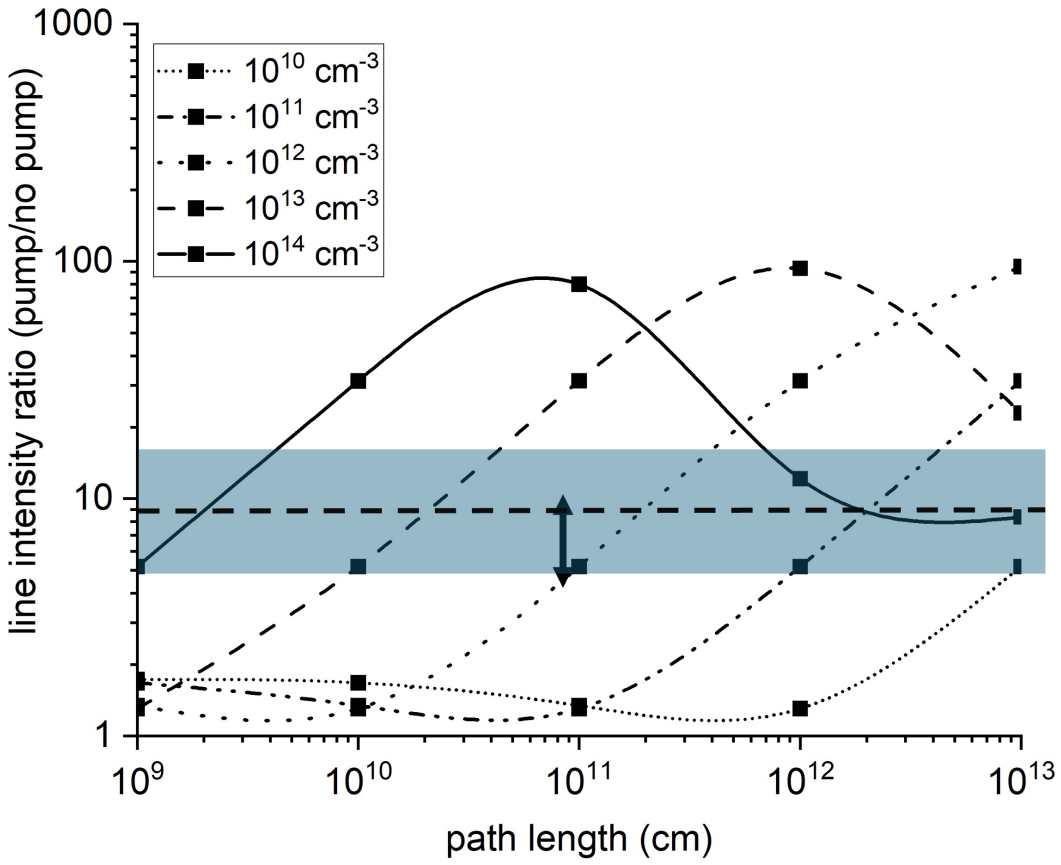

Figure 4. Plot of the enhancement factor (i.e. line intensity of the photopumped line divided by that when there is no pumping) for the 82.76 Å line of Ne IX as a function of pathlength L for a range of electron densities N_e, at the electron temperature of maximum Ne IX fractional abundance in ionization equilibrium, $T_e = 1.6\times10^6$ K (Bryans et al. 2009). The decrease in enhancement at large L and N_e is due to the onset of opacity in the 82.76 Å line. Also shown in the figure is the measured enhancement factor of 7 ± 3, indicated by a dashed line with the error bar as the shaded region, plus the theoretical value of 5 – 16 plotted as a vertical arrow at log L = 10.9.

4.2. *Electron density estimate*

Clearly, the best electron density diagnostic for an Ne IX-emitting plasma is the well-known Ne IX forbidden (f) to intercombination (i) line intensity ratio (Gabriel & Jordan 1969), but in flaring plasmas the f and i lines are blended with strong Fe XIX transitions (Bhatia et al. 1989). We do detect the O VII f and i lines in HR 1099, with a ratio of f/i = 2.3 ± 1.8, which from CHIANTI indicates log $N_e = 10.3^{+0.9}_{-2.3}$. However, this ion is formed at only log $T_e = 5.9$ (Bryans et al. 2009), somewhat further away from Ne IX (log $T_e = 6.2$) than Mg XI (log $T_e = 6.4$). Hence, we believe

that the Mg XI f/i ratio is probably the most suitable alternative diagnostic for the Ne IX region. Unfortunately, the Mg XI components were not well detected in our flare spectrum, with only an upper limit for the intercombination lines at 9.23 Å. Combined with the forbidden line at 9.31 Å this yields a ratio f/i > 0.53, which from CHIANTI indicates log $N_e < 13.4$. However, Testa et al. (2004) measured Mg XI electron densities for HR 1099 from both Chandra Medium Energy Grating (MEG; 2.5 – 31 Å) and High Energy Grating (HEG; 1.2 – 15 Å) spectra. They found log $N_e = 12.3^{+0.1}_{-0.2}$ and $12.5^{+0.3}_{-0.5}$ for their MEG and HEG observations, respectively. We show the O VII and Mg XI line regions in Figure 6. There are additional N_e-diagnostics in the 22 – 75 Å region listed by Brown et al. (1986), but unfortunately none are detected by us. In any event these diagnostics appear to become N_e-insensitive for log $N_e >$ 11, so would not be useful for diagnosing a higher electron density stellar flare plasma. Given the above, based on the Mg XI results of Testa et al. (2004) we adopt a density of log $N_e = 12.3 - 12.5$ for our Chandra flare spectrum of HR 1099.

4.3. *Photopumping of Ne IX*

From Table 2 the Ne IX intensity ratio 82.76 Å/13.45 Å $= 0.21 \pm 0.08$. However, the theoretical ratio from CHIANTI is only 0.031 for the AU Mic and flare EMD models, near the high temperature limit of 0.033, and has an even smaller value of 0.019 for the isothermal case. This indicates an enhancement in the 82.76 Å line of at least a factor of ∼7 ± 3. As noted above, we have adopted an electron density of log $N_e = 12.3 - 12.5$ for the Ne IX-emitting region of the HR 1099 flare. Unfortunately, we have no information on the loop geometry and hence the best we can do is adopt the loop pathlength range (in cm) for HR 1099 of log L = 10.7 – 11.1 derived by Mullan et al. (2006) using the Haisch Simplified Approach (Haisch 1983). Such pathlength values imply much larger emission measures for the star than previously derived by, for example, Huenemoerder et al. (2013). However, we note that we may be observing the loop along its length, and indeed we discuss below how the detection of line enhancement may provide geometrical information on coronal loops in spatially unresolved sources. In addition, if the emission measure is as large as our adopted values of N_e and L imply, then one might expect to see resonance scattering in the O VIII Lyα line, as found by Testa et al. (2004). We have detected both Lyα 18.97 Å and Lyβ 16.00 Å in our HR 1099 flare spectrum, shown in Figure 6. However, Lyβ is blended with Fe XVIII 16.00 Å, with the CHIANTI models indicating a Fe XVIII 16.00/16.08 ratio of about 0.70 for both the AU Mic and flare EMDs, implying that Fe XVIII makes a contribution of 21×10^{-5} ph cm^{-2} s^{-1} to the total 16.00 Å flux. This in turn yields a measured Lyα/Lyβ ratio of 6.3 ± 0.9, compared to a minimum theoretical value of 7.6 from CHIANTI, indicating significant resonance scattering in Lyα, confirming that the HR 1099 flare plasma must indeed have high N_e and L.

For the above values of N_e and L we calculate an enhancement factor of 5 – 16, in agreement with measurement, as shown in Figure 4. Even if we adopt the lower limit value of log L = 10.7, this still implies an enhancement factor of ∼8, and we note that Strassmeier & Bartus (2000) calculated a loop pathlength of log L = 10.7 for HR 1099 based on Doppler imaging observations. Given this, we believe our result confirms the occurrence of X-ray line coincidence photopumping in HR 1099 during a flare, previously only very marginally identified in a solar flare spectrum by Keenan et al. (2018). We also note that, although we compare our LETG flare spectra to previous solar flare observations (Acton et al. 1985; Phillips et al. 1982; Keenan et al. 2018), our CHIANTI models are not based on solar flare data. They have been generated for a highly active late-type star differential emission measure appropriate to HR 1099, and with the HR 1099 abundances, as discussed in Section 3.

As detailed in Keenan et al. (2018), the determination of stellar flare loop pathlengths requires various assumptions to be made, so the detection of line enhancement provides in principle a powerful tool to independently measure L and (in the case of flare stars) magnetic field strength. In addition, it could be employed to determine a plasma pathlength in any remote astrophysical source with similar N_e and L values to flares, such as AGN coronal regions (Reeves et al. 2016). With this in mind, we plan to extend our work in two ways. First we will search the Chandra and additional suitable databases for the spectra of sources other than late-type flare stars to search for evidence of X-ray photopumping of Ne IX. Secondly, we will investigate other possible coronal photopumping schemes, important to show that the Ne IX case is not unique and may be a common occurrence. A particularly promising one involves H-like Ne X 12.13 Å pumping Ne-like Fe XVII 12.13 Å, leading to predicted enhancement in Fe XVII lines between 204 – 389 Å (Nilsen & Chandler 1991).

Table 2. Measured LETG lines and parameters for HR 1099

Energy	Wavelength		Line Flux[a]				ID	Comment
(keV)	Observed	Lab[b]	Flare		Quiet			
(keV)	(Å)	(Å)	Flux	Error	Flux	Error		
0.0933	132.92	132.91	1021.8	92.5	680.8	35.2	Fe XXIII/Fe XX	DZ13, blend
0.0963	128.78	128.75	200.3	50.1	220.1	22.2	Fe XXI	DZ13
0.1058	117.19	117.17	239.1	40.4	170.8	15.5	Fe XXII	M01
0.1193	103.93	103.95	70.3	28.2	47.3	10.5	Fe XVIII	K74, blend?
0.1320	93.95	93.94	153.0	44.6	117.2	10.7	Fe XVIII	A85, K74, blend?
0.1459	84.98	85.02	27.4	16.2	10.4	5.4	Zn XXIII	W88
0.1498	82.76	82.76	33.4	11.9	<12	...	Ne IX	K18
0.1871	66.26	66.25	33.7	19.4	17.6	5.6	Fe XVI	K06
0.1888	65.66	65.66	36.4	16.2	15.3	5.5	Mg X	A85
0.2091	59.30	59.40	25.1	13.1	56.1	8.2	Fe XV	K06
0.2177	56.95	56.95	39.6	18.0	6.1	5.0	C VI	A85
0.5605	22.12	22.10	43.0	17.1	28.6	6.4	O VII	A85
0.5683	21.82	21.81	18.8	12.8	12.2	4.7	O VII	M01
0.5732	21.63	21.60	46.8	17.1	64.3	7.4	O VII	A85
0.6530	18.99	18.97	528.0	24.3	395.4	9.9	O VIII	Lyα, *A*85
0.7250	17.10	17.07	88.8	18.4	120.5	8.0	Fe XVII	A85, blend
0.7380	16.80	16.78	53.6	11.6	48.3	4.7	Fe XVII	A85
0.7696	16.11	16.08	29.7	10.4	28.5	6.2	Fe XVIII	A85
0.7735	16.03	16.00	105.2	14.1	91.4	8.3	O VIII	Lyβ, *A*85
0.8250	15.03	15.01	95.3	13.1	88.8	5.5	Fe XVII	A85
0.9050	13.70	13.70	69.8	12.1	60.2	4.9	Ne IX	f, A85
0.9150	13.55	13.55	28.8	11.1	44.3	4.7	Ne IX	i - blended, A85
0.9200	13.48	13.45	162.5	15.8	110.9	6.0	Ne IX	r, A85
0.9560	12.97	12.97	20.6	10.1	26.7	4.1	Fe XX	CH
0.9633	12.87	12.85	19.1	13.7	21.0	4.9	Fe XX	A85
0.9666	12.83	12.82	41.2	15.3	26.4	4.8	Fe XX/Ni XIX	A85
1.0208	12.15	12.12	442.6	22.1	296.9	8.6	Ne X	Lyα, *A*85
1.0380	11.94	11.94	12.2	9.4	6.5	3.4	Fe XXII	P82
1.0540	11.76	11.77	64.3	11.8	54.9	4.7	Fe XXII	P82
1.0970	11.30	11.32	6.3	9.5	5.8	3.4	Fe XVIII	P82
1.1070	11.20	11.25	11.6	9.8	20.2	3.9	Fe XVII/Fe XVIII	P82
1.1240	11.03	11.00	54.7	11.7	28.8	4.2	Ne IX/Na X	P82
1.1478	10.80	10.77	19.2	9.9	1.4	3.1	Fe XVII/Ne IX	P82
1.1630	10.66	10.66	36.2	10.6	17.4	3.8	Fe XIX	P82

Table 2 *continued on next page*

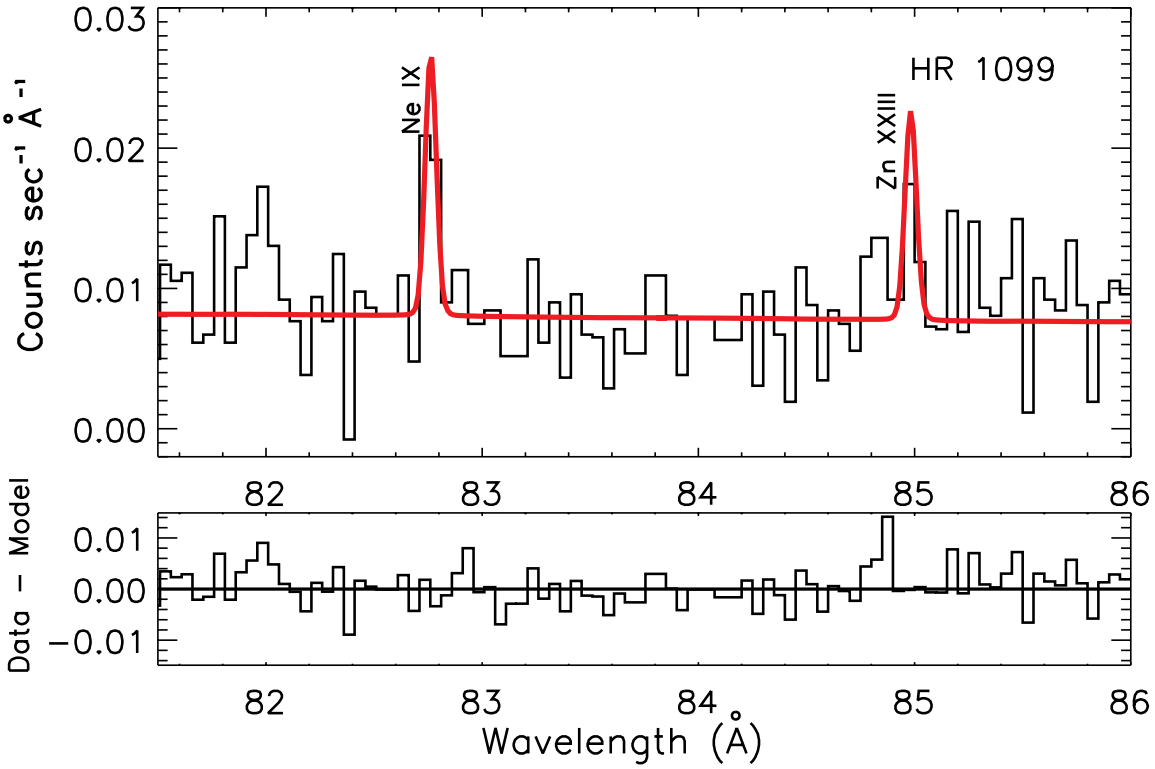

Figure 5. Expanded view of the 80–90 Å region for the HR 1099 flare spectrum, showing the Ne IX 82.76 Å and Zn XXIII 85.02 Å lines. The spectrum is plotted as a black histogram, and the best-fitting emission line model as a red curve. The lower panel plots a histogram of the residuals of the measurements minus the model.

Table 2 *(continued)*

Energy	Wavelength		Line Flux[a]				ID	Comment
(keV)	Observed	Lab[b]	Flare		Quiet			
(keV)	(Å)	(Å)	Flux	Error	Flux	Error		
1.2780	9.70	9.71	11.0	8.9	8.2	3.3	Ne X	P82
1.3346	9.29	9.31	14.9	10.1	3.6	3.4	Mg XI	f, P82
1.3440	9.22	9.23	<28		4.2	3.1	Mg XI	i, P82
1.3520	9.17	9.17	17.8	9.8	16.0	3.5	Mg XI	r, P82
1.8560	6.68	6.68	38.7	7.8	20.1	2.7	Si XIII	P82

[a]Line flux in 10^{-5} ph $cm^{-2}s{-}1$; < denotes a 3-*sigma* upper limit.
[b]Laboratory wavelength reference is given in comments, with A85=Acton et al. (1985); CH = CHIANTI, Dere et al. (1997, 2023); DZ13=Del Zanna & Woods (2013); K74=Kastner et al. (1974); K06 =Keenan et al. (2006); K18=Keenan et al. (2018); M01 = Mewe et al. (2001); P82=Phillips et al. (1982); W88=Wouters et al. (1988).

ACKNOWLEDGMENTS

This research was supported by NASA Chandra grant AR9-20001X and the United Kingdom Science and Technology Facilities Council via grant ST/T00021X/1. This research has made use of data obtained from the Chandra Data Archive provided by the Chandra X-ray Center (CXC). CHIANTI is a collaborative project involving George Mason University, the University of Michigan (USA), University of Cambridge (UK) and NASA Goddard Space Flight Center

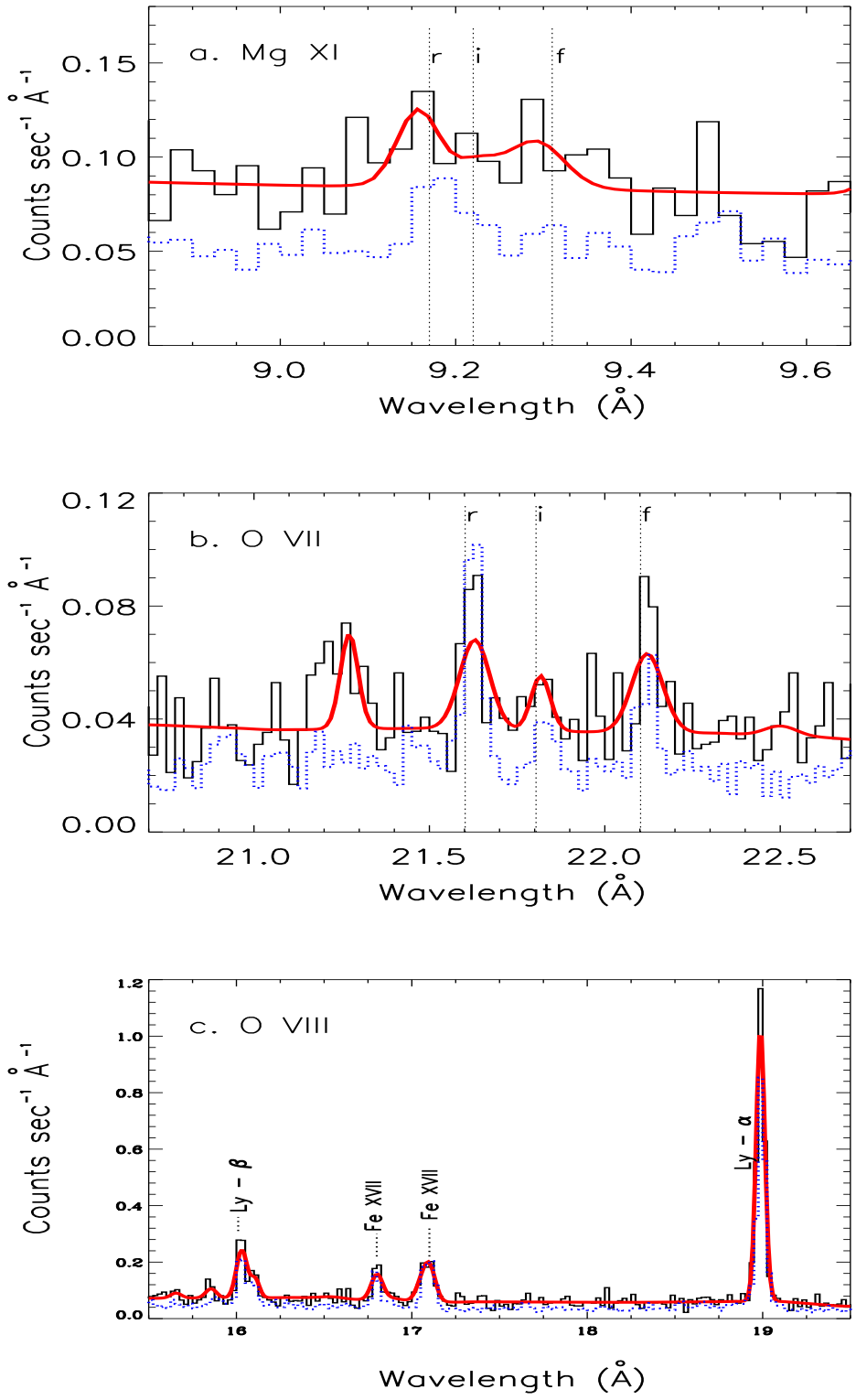

Figure 6. Expanded view of spectral regions for the density diagnostics discussed in Section 4.2, with (a) the 9–10 Å region for Mg XI and (b) the 21–22 Å region for O VII. Also shown in the figure (panel c) is the 16–19 Å region for O VIII Lyα and Lyβ, discussed in Section 4.3. Data are plotted as black histograms, and the best-fitting emission line model over-plotted as red curves. The quiescent spectrum is also over-plotted as blue histograms (dotted-line).

(USA). We thank the Oxford University Press and Monthly Notices of the Royal Astronomical Society for copyright permission to reuse Figure 1 from Keenan et al. (2018). We thank an anonymous referee for suggested improvements to the manuscript.

Facilities: CXO

Software: CIAO 4.16

REFERENCES

Acton, L. W., Bruner, M. E., Brown, W. A., et al. 1985, Astrophysical Journal, 291, 865

Bhatia, A. K., Fawcett, B. C., Phillips, K. J. H., Lemen, J. R., & Mason, H. E. 1989, Monthly Notices of the Royal Astronomical Society, 240, 420

Bowen, I. S. 1934, Publications of the Astronomical Society of the Pacific, 46, 207

Brinkman, A. C., Gunsing, C. J. T., Kaastra, J. S., et al. 2000, Astrophysical Journal, 530, 111

Brinkman, A. C., Behar, E., Güdel, M., et al. 2001, A & A, 365, L324

Brown, W. A., Bruner, M. E., Acton, L. W., & Mason, H. E. 1986, Astrophysical Journal, 301, 981

Bryans, P., Landi, E., & Savin, D. W. 2009, Astrophysical Journal, 691, 1540

Del Zanna, G., & Woods, T. N. 2013, Astronomy & Astrophysics, 555, A59

Dere, K. P., Del Zanna, G., Young, P. R., & Landi, E. 2023, Astrophysical Journal Supplement Series, 268, 52

Dere, K. P., Landi, E., Mason, H. E., Monsignori Fossi, B. C., & Young, P. R. 1997, A & A Supplement series, 125, 149

Fruscione, A., McDowell, J. C., Allen, G. E., et al. 2006, SPIE, 6270, 62701V

Gabriel, A. H., & Jordan, C. 1969, Monthly Notices of the Royal Astronomical Society, 145, 241

Haisch, B. M. 1983, IAU Colloq. 71: Activity in Red-Dwarf Stars, 102, 255

Hartman, H. 2013, in Springer Series on Atomic, Optical and Plasma Physics, ed. M. Mohan, 76, 189

Hilton, E. J., West, A. A., Hawley, S. L., , & Kowalski, A. F. 2010, Astronomical Journal, 140, 1402

Huenemoerder, D. P., Phillips, K. J. H., Sylwester, J., & Sylwester, B. 2013, Astrophysical Journal, 768, 135

Hussain, G. A. J., Jardine, M., Donati, J. F., et al. 2007, Monthly Notices of the Royal Astronomical Society, 377, 1488

Kastner, S. O., Neupert, W. M., & Swartz, M. 1974, Astrophysical Journal, 191, 261

Keenan, F. P., Drake, J. J., Chung, S., et al. 2006, Astrophysical Journal, 645, 597

Keenan, F. P., Poppenhaeger, K., Mathioudakis, M., et al. 2018, Monthly Notices of the Royal Astronomical Society, 474, 3782

Lemen, J. R., Title, A. M., Akin, D. J., et al. 2012, Solar Physics, 275, 17

Mewe, R., Raassen, A. J. J., J, D. J., et al. 2001, Astronomy & Astrophysics, 368, 888

Mullan, D. J., Mathioudakis, M., Bloomfield, D. S., & Christian, D. J. 2006, Astrophysical Journal Supplement Series, 164, 173

Ness, J. U., Schmitt, J. H. M. M., Burwitz, V., et al. 2002, A & A, 384, 911

Nilsen, J., & Chandler, E. 1991, Phys. Rev A., 44, 4591

Nordon, R., & Behar , E. 2007, A&A, 464, 309

Phillips, K. J. H., Aggarwal, K. M., Landi, E., & Keenan, F. P. 2010, A&A, 518, A41

Phillips, K. J. H., Fawcett, B. C., Kent, B. J., et al. 1982, Astrophysical Journal, 256, 774

Reeves, J. N., Porquet, D., Braito, V., et al. 2016, Astrophysical Journal, 828, 98

Strassmeier, K. G., & Bartus, J. 2000, A & A, 354, 537

Testa, P., Drake, J. J., & Peres, G. 2004, Astrophysical Journal, 617, 508

Walter, F., Bowyer, S., & Charles, P. 1978, Nature, 274, 569

Wouters, A., Schwob, J. L., S. Suckewer, S., et al. 1988, Optical Society of America, 5, 1520